Appl. Phys. A 68, 197–201 (1999)

Applied Physics A
Materials
Science & Processing

Nanostructures produced by cluster beam lithography

A. Gruber, J. Gspann, H. Hoffmann

Universität Karlsruhe und Forschungszentrum Karlsruhe, Institut für Mikrostrukturtechnik, Postfach 3640, D-76021 Karlsruhe, Germany
(Fax: +49-7247/82-4331)

Received: 3 July 1998

Abstract. Accelerated ionized cluster beams are used for surface nanostructuring of bulk diamond, CVD diamond films, single-crystalline silicon, or glass, via reactive accelerated cluster erosion (RACE). Beams of CO_2 clusters with about 1000 molecules per unit charge are accelerated to up to 120 keV kinetic energy for mask projective surface bombardment. Patterning is achieved via physical as well as chemical surface erosion. Very smooth eroded surfaces result for bulk natural diamond, silicon, and glass. Polycrystalline, strongly faceted CVD diamond films are effectively planarized. Submicron structures with various wall inclinations can be generated. Atomic force microscopy of individual impact structures reveals nanometer-sized hillocks instead of craters. The collective motion of the impacted surface material is considered crucial for the cluster impact-induced nanomodifications. Atomic ion beam lithography is considered for comparison.

PACS: 36.40; 68.35; 81.65

Beams of nanoparticles, or clusters of atoms or molecules, can be used for deposition of materials onto surfaces, for modifying surfaces by mixing or chemical transformation, and for eroding surfaces physically or chemically. Increasingly larger impact energies are required for the respective processes in the cited order. While the main topic of the present contribution is the structure generation by mask projective erosion, especially by reactive accelerated cluster erosion (RACE) [1], it should be mentioned that ionized-cluster beam (ICB) deposition [2] has a long and strongly debated history in thin film generation. The authors' group succeeded in generating intense beams of neutral clusters from pure vapor nozzle expansions of cesium, zinc, silver, and, for periods of minutes, of gallium [3], using feed vapor pressures in the range of a few bar. However, broad beam ionization and acceleration of such high-intensity metal beams has still to be achieved in order to realize in full the original ICB deposition concept. Furthermore, materials of lower vapor pressure, such as most metals, cannot be vaporized thermally to sufficiently high source pressures. However, if isolated nanoparticle deposition is the main goal, high-intensity cluster beams may not be required, and other types of cluster beam sources using laser, plasma, spark, or sputter vaporization of cluster material into some carrier gas may be well suited.

Gas cluster beams, on the other hand, can easily be obtained from high-density source gas conditions [4], as investigated in depth for nuclear fusion purposes [5], so that intense cluster beams for surface modification or erosion are readily available. With respect to micro- or nanostructuring, however, one has to take into account that the distribution of cluster sizes from such nozzle sources is never narrow, usually following a log–normal distribution [6], while the velocity distribution is rather monochromatic. Hence, the distribution of cluster masses leads to a corresponding distribution of the kinetic energies of the neutral clusters as they leave the nozzle. As these energies are of the order of 100 eV or more, they are not negligible in comparison with the energies obtained by electrical acceleration, thus preventing a really fine focusing. For example, puncturing a 50-μm-thick W foil by a CO_2 cluster beam of 155 keV, "focused as well as possible", led to a hole of 0.13 mm diameter [7].

By contrast, using isotopically pure gallium in a liquid metal ion source, a minimum spot size of a focused ion beam (FIB) of 8 nm has been reported [8]. Other ion beam columns have been equipped with a Wien filter for ion mass separation in order to obtain submicron resolution [9]. Thus, ionized cluster beams without a mass separation cannot compete with atomic ion beams in the focused ion beam mode with respect to spatial resolution. Focused (atomic) ion beam writing can be used for direct machining, for example in mask repair, as well as for maskless, software-controlled resist exposure, where the main advantages are the small sidewise exposure of the resist due to low-energy secondary electrons, and negligible ion straggling and backscattering. As ion beam writing is a slow sequential process, however, ion projection lithography is developed for parallel resist exposure using flood illumination of masks and electrostatic ion optics for pattern scale reduction. This latter feature, in particular, makes ion projection lithography interesting for future IC fabrica-

tion [10]. Again, however, single-mass ions are needed to achieve 10 to 100 nm resolution. Hence, cluster beams do not qualify for this technique either.

The present paper describes a direct machining by accelerated ionized clusters which are flood-illuminating a mask in close proximity to the workpiece. Thus the fineness of the pattern is completely determined by the mask which is 1 : 1 projected. The technique is distinguished by very smooth eroded surfaces [7]. Clusters of, on the average, 1000 molecules of CO_2 or SF_6 are accelerated to 100 keV. The impact of these clusters creates very high energy densities in the impact region, resulting in a plasma of cluster and surface material that allows chemical reactions to occur. Volatile reaction products may be formed, which relieves the debris problem. Hence, the technique is called reactive accelerated cluster erosion (RACE). The term "erosion" is preferred over "sputtering" in order to underline the specific character of the cluster impact, which involves collective motions of projectile and target material. In the following, after a short description of the experimental facility, examples of mask projective cluster micromachining are presented. While this structuring requires prolonged cluster bombardment, the effects of individual accelerated cluster impacts are studied by atomic force microscopy of short-time exposed surfaces. The lateral extension of these impact effects determines the final lateral resolution of the cluster beam lithography and is found to be of the order of several 10 nm.

1 Experimental

Cluster lithography is effected using beams of electrically accelerated ionized clusters in a shower beam mode and suitable stencil masks. The clusters are generated by adiabatic nozzle expansion of CO_2 or SF_6 gas, the converging–diverging nozzle having 0.1 mm throat diameter, 10° angle of initial divergence, and 28 mm length of the divergent part (Fig. 1). Most of the expanding gas is frozen onto cryopanels attached to a liquid nitrogen bath cryostat. The core of the expanding nozzle flow is transferred to high vacuum via two skimming orifices. Electrons of 150 eV energy partly ionize the cluster beam, which may then be focused by up to 10 kV potential negative with respect to the acceleration potential [11].

The cluster mean sizes can be measured by using a dedicated time-of-flight spectrometer in place of the target [12]. The nozzle feed pressure is chosen to provide clusters of a suitable size, for example 1000 molecules of CO_2 per unit charge, in order to ensure high-speed impacts. At the chosen 100 kV acceleration voltage the ionized clusters impinge on the target with a speed of about 20 km/s.

The experimental setup described earlier [11] is now equipped with a rapid beam shutter which allows times of exposure as short as 0.5 ms. A manually operated additional beam flag serves to protect the rapid shutter from prolonged cluster beam erosion. Target, mask, and beam shutters are all kept at ground potential. The cluster beam source can be operated at high potential of either polarity. In the present case, a positive potential of 100 kV is used to accelerate positive cluster ions towards the ground electrode, which they pass via a 100-mm-diameter central orifice.

Most often, a microstructured nickel foil of 8 μm thickness, which is generated via e-beam lithography and nickel galvanoforming, serves as a stencil mask. Its proximity distance from the target is of the order of 50 μm, as obtained by optical microscope inspection.

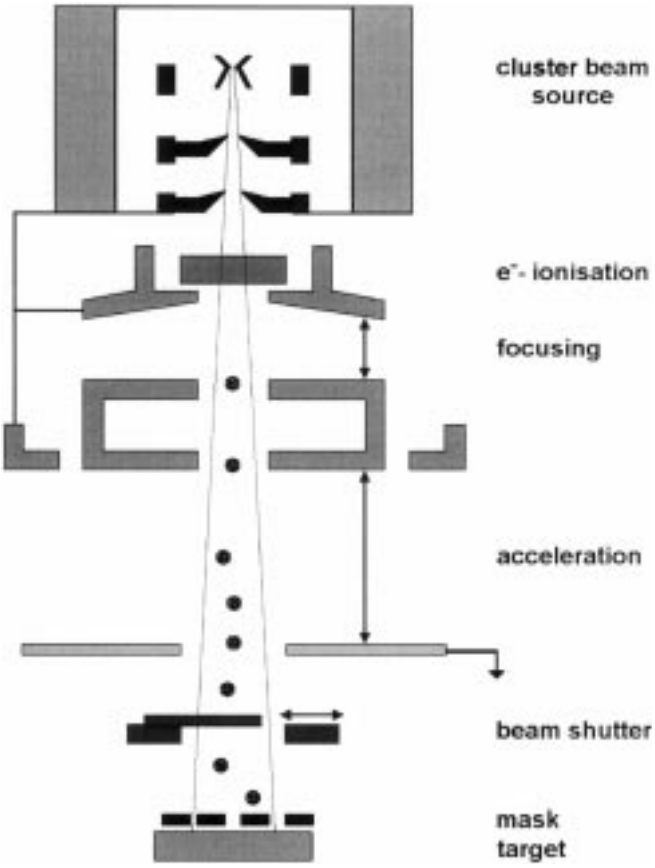

Fig. 1. Schematic view of the setup for reactive accelerated cluster erosion (RACE)

After exposure to the accelerated ionized cluster beam, the targets are transferred through ambient atmosphere without particular precautions to either a scanning electron microscope (SEM) or a Digital Instruments Nanoscope III. They are investigated by atomic force microscopy (AFM) in the so-called contact mode using silicon nitride cantilevers, or in the tapping mode with Si cantilevers.

2 Results

2.1 Cluster-eroded microstructures

2.1.1 Glass and quartz. Figure 2 shows hexagonal blind holes eroded by impact of CO_2 clusters of about 1000 molecules into Pyrex glass using a nickel mask at about 50 μm distance from the target surface [1]. According to the SEM micrograph the bottom planes are at least as smooth as the original glass surface. In spite of the large proximity distance, steep sidewalls are achieved due to the rather parallel cluster trajectories. Some vertical striations may be seen in the sidewalls of the blind holes, which at least in part result from corresponding structures of the mask.

Figure 3 shows a similar blind hole eroded into polycrystalline quartz. Obviously, the process of cluster erosion leads

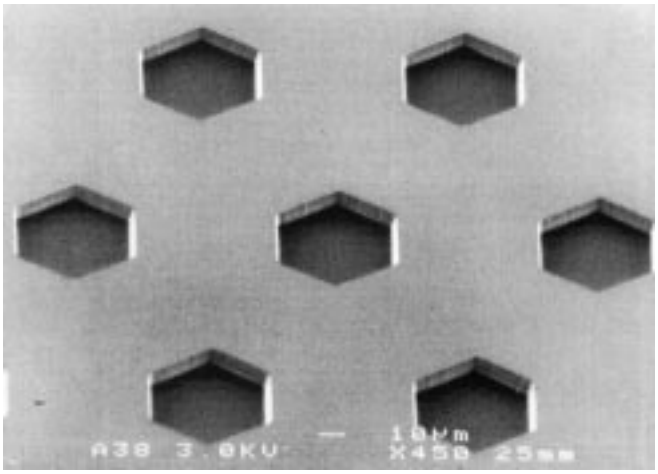

Fig. 2. Blind holes eroded into Pyrex glass by CO_2 clusters

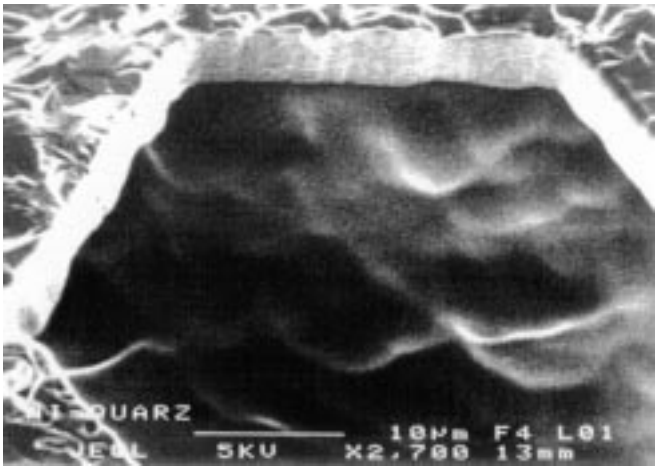

Fig. 3. Blind hole eroded into polycrystalline quartz by CO_2 clusters

to a smoothening of the eroded surface which is reminiscent of melting at the surface of the target. In the sidewalls no vertical, but horizontal, striations may be recognized. This type of striation is also observed regularly with metal targets, such as gold or copper. The striations are found to remain horizontal even when the target is tilted against the vertical direction. Hence, they may be due to a thin layer of fluid which freezes onto the sidewalls, showing surface ripples oriented perpendicular to the gravity direction.

2.1.2 Diamond. The result shown in Fig. 3 motivated the use of cluster erosion also for planarizing polycrystalline artificial diamond films [13]. Figure 4 gives an example of a part of a hexagon eroded into diamond film which had been deposited by chemical vapor deposition (CVD).

The very pronounced smoothing achieved is similar to the results obtained with quartz (Fig. 3), again indicating some kind of superficial melting. The underlying crystal structure can still be recognized in the residual, mostly triangular holes.

Originally, the films were black due to a residual graphitic component which also makes the films conducting. In the scanning electron microscope, these films appear bright. The eroded parts, however, show up black in the SEM due to lost conductivity, but nearly white under natural illumination.

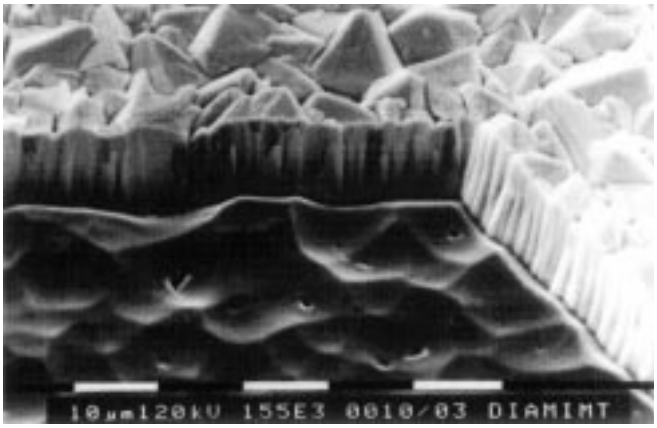

Fig. 4. Artificial polycrystalline diamond film partially planarized by accelerated CO_2 cluster bombardment

Obviously, the chemical reaction with the CO_2 clusters has preferentially removed the graphitic component.

2.2 Individual impact patterns

Reducing the time of exposure of the target by use of the rapid beam shutter allowed us to identify isolated impact structures, as shown in Fig. 5 for silicon [14]. Commercial polished Si(100) wafers have been selected as targets because of their original flatness. The impact structures turn out to be always hillocks, the areal density of which corresponds to the areal density of cluster impacts. The hillocks came as a surprise since craters were expected [15].

Another illustrative example of an impact structure is presented in Fig. 6. Here, a crown of hillocks surrounds a higher central peak. The height of this central elevation is truncated in Fig. 6, its true value being 2 nm according to a corresponding height profile.

A final example of an impact-induced pattern is given in Fig. 7. Although such pyramids have also been seen on silicon substrates, Fig. 7 has been obtained with a Pyrex glass target.

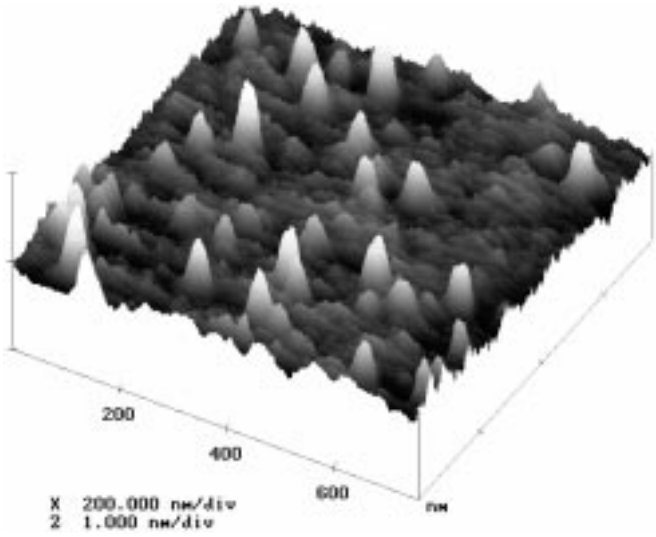

Fig. 5. Atomic force micrograph of isolated impact-induced hillocks on a Si wafer surface

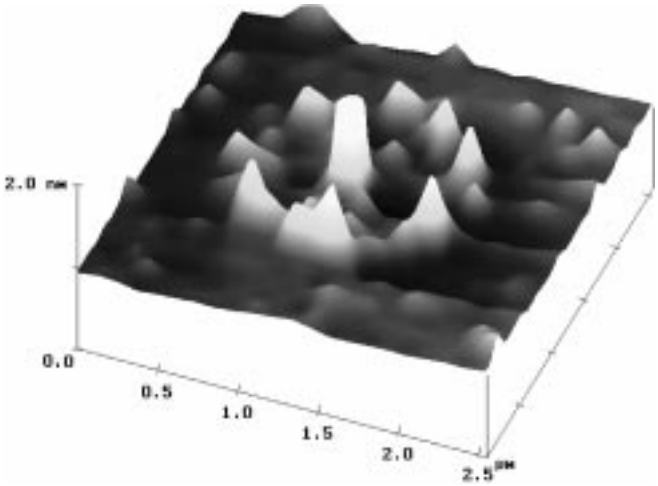

Fig. 6. AFM image of an impact-induced peak with surrounding hillock crown on a Si wafer

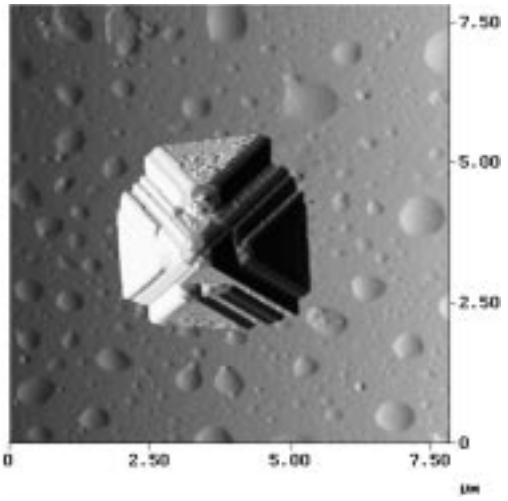

Fig. 7. Impact-induced elevated structure on a Pyrex glass surface as recorded by the atomic force microscope with a pyramidal tip

The frequency of these large pyramidal structures is about a factor 1500 lower than that of the ones shown in Fig. 5. The small crown of Fig. 6 seems to be a very rare event as it is the only one of its kind found up to now. At the moment, the origin and the specifications of the projectiles responsible for the patterns of Figs. 6 and 7, such as mass and charge state, are not known.

3 Discussion

From macroscopic ballistic experiments it is known that hypervelocity impacts of spherical projectiles invariably yield hemispherical surface craters whose volume is proportional to the impact energy [16]. Extrapolating these results to the impacts of clusters of 100 keV impact energy leads to predicted crater diameters of some ten nanometers, which are considerably larger than the average diameter of about 3 nm of the impinging clusters [15]. Although the lateral dimensions of the observed hillocks correspond approximately to the expected crater diameters, elevations instead of excavations never show up in the macroscopic ballistic experiments. It also has to be recalled that prolonged bombardment leads to erosion of material, not deposition.

The average roughness of the sample first increases with the number of isolated hillocks, then decreases when the gaps between hillocks fill up, and finally increases again to less than 0.5 nm. Auger electron spectroscopy reveals that elements of the cluster material, i.e. C and O, can be found down to depths of 20 nm [17]. This depth corresponds roughly to the expected crater depths.

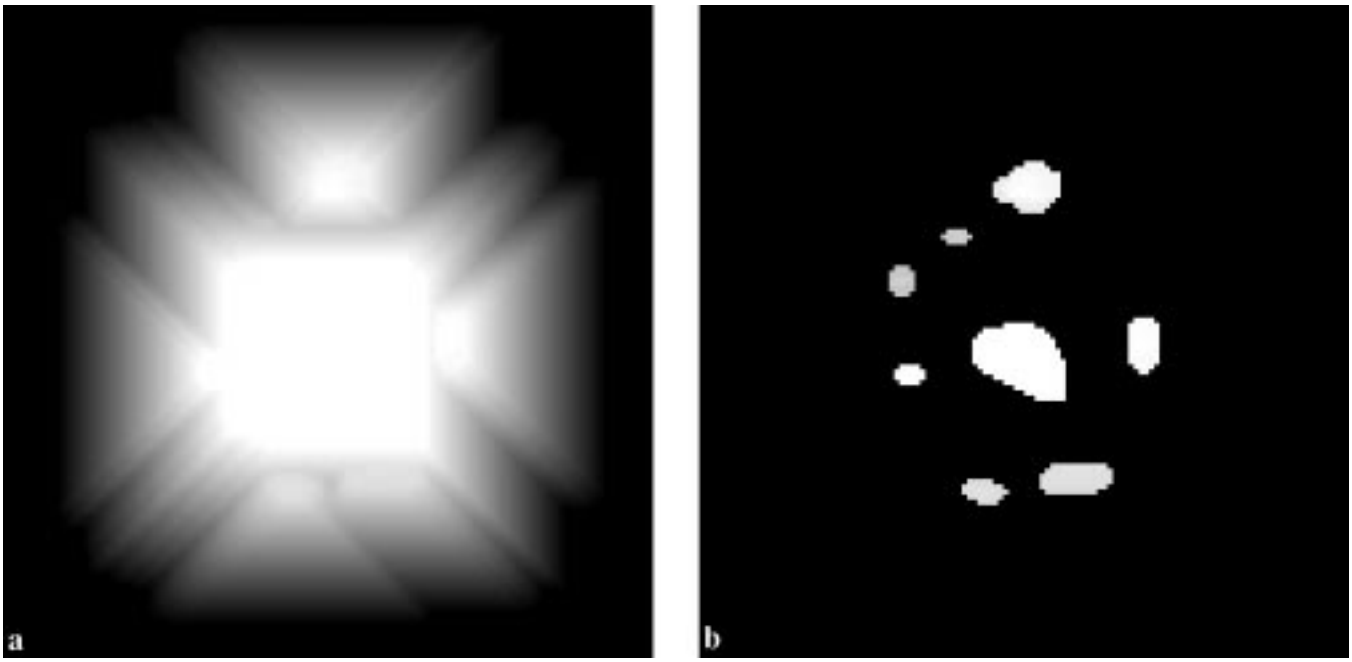

Fig. 8a,b. Side-structured pyramid (**a**) simulating the one in Fig. 7 by convolution of the typical AFM tip topology with an assumed centered peak crown (**b**). The image size is 3.8 µm × 3.8 µm, the central peak is 1.7 µm high

The features in Fig. 6 bear a strong resemblance to the transitory splashing patterns following the impact of a projectile onto a liquid surface. Considering the whole crown pattern of Fig. 6 as a consequence of a single impact, the projectile must have been much larger and more energetic than the ordinary cluster impact structures of Fig. 5. These latter ones could perhaps represent central peaks, the hillock crowns of which are too low to be detected.

On the other hand, the pattern of Fig. 7 has to be ascribed to an even more energetic projectile, regarding the size of the affected area. As the structure on the target surface obviously is of considerable height, about 1.7 μm, one has to take into account the possibility of the target structure probing the tip of the microscope, instead of vice versa. Indeed, the inclinations of the side planes of the pyramid agree with the angles of inclinations resulting from anisotropic wet etching of single-crystalline Si, as is used for producing the cantilever tips. Pyramid topologies vary between samples, possibly due to variations of the respective cantilever tips. Figure 8 shows a crown pattern with a central peak which yields an atomic force microscopy result such as the one given in Fig. 7 when convoluted with the typical topology of the atomic force microscope tip, viz., a pyramid with an apex angle of 70°.

The impact-induced structures shown in Figs. 5–7 all show elevated patterns which indicate transient localized surface melting of the target material. Apparently, initially formed craters collapse due to too slow a heat removal. The origin of the projectiles larger than 1000 molecule clusters has still to be investigated. In agreement with expectations, however, the most frequent ionized cluster impacts affect areas of some ten nanometer diameter per impact.

The low height of the cluster impact-induced hillocks, on the other hand, explains the remarkable smoothness of the cluster-eroded surfaces. This has to be compared with the "grass-like" patterns often observed with atomic-ion sputtering [18]. Such an appearance has never been found with cluster erosion, presumably due to the collective lateral movement of the eroded material, which prevents or destroys the buildup of needle-like structures. Centered peak crowns such as the ones shown in Figs. 6 and 8, on the other hand, can be found only after short times of exposure, 0.1 ms or less, which indicates a generation by a single energetic impact event.

4 Conclusion

Ionized cluster beams accelerated to kinetic energies of the order of 100 eV per constituent cluster molecule can be used for micromachining surfaces of all materials by reactive accelerated cluster erosion (RACE). Using gases, such as CO_2 or SF_6, as a starting material ensures cluster formation will occur in sufficiently dense adiabatic nozzle expansions. On the other hand, the high impact energies lead to disintegration even of the molecular constituents, so that chemical reactions become possible, which may lead to volatile products, or to surface modification. Individual impacts affect surface areas of several 10 nm diameter. Single mass atomic ion beams can be focused to give comparable spot sizes, which is not possible with the present cluster beam setup without installing a cluster mass filter.

It is observed that prolonged bombardment with accelerated clusters yields smooth eroded surfaces whereas individual impacts lead to hillocks of less than 1 nm height, if the projectiles are 1000-molecule CO_2 clusters. These hillocks are assumed to result from the relaxation of transitory craters by an elastic rebound of molten surface material.

Acknowledgements. The authors gratefully acknowledge fruitful discussions with L.P. Biró, P. von Blanckenhagen, and B. Ivanov.

References

1. J. Gspann: Microelectron. Eng. **27**, 517 (1995)
2. T. Takagi: *Ionized-cluster Beam Deposition and Epitaxy* (Noyes Publications, New Jersey 1988)
3. J. Gspann: Laser and Ion Beam Modification of Materials, ed. by I. Yamada et al., Trans. Mater. Res. Soc. Jpn., Vol. 17 (Elsevier Science, Amsterdam 1994) pp. 107–110
4. E.W. Becker, K. Bier, W. Henkes: Z. Phys. **146**, 333 (1956)
5. E.W. Becker: Laser Part. Beams **7**, 743 (1989)
6. J. Gspann, H. Vollmar: *Rarefied Gas Dynamics*, ed. by K. Karamcheti (Academic Press, New York 1974) pp. 261–268
7. P.R.W. Henkes, R. Klingelhöfer: J. Phys. (Paris) **50:C2**, 159 (1989)
8. J. Orloff: Rev. Sci. Instrum. **64**, 1105 (1993)
9. T. Shiokawa, P.H. Kim, K. Toyoda, S. Namba: J. Vac. Sci. Technol. B **1**, 1117 (1983)
10. G. Stengl, H. Löschner, W. Maurer, P. Wolf: J. Vac. Sci. Technol. B **4**, 194 (1986)
11. J. Gspann: Surf. Rev. Lett. **3**, 897 (1996)
12. J. Gspann, H. Vollmar: J. Chem. Phys. **73**, 1657 (1980)
13. J. Gspann: Sens. Actuators A **51**, 37 (1995)
14. P. von Blanckenhagen, A. Gruber, J. Gspann: Nucl. Instrum. Methods Phys. Res., Sect. B **122**, 322 (1997)
15. J. Gspann: In *From Clusters to Crystals*, ed. by P. Jena et al. (Kluwer, Amsterdam 1992) pp. 115–1120
16. J.J.W. Gehring: In *High-Velocity Impact Phenomena*, ed. by R. Kinslow (Academic Press, New York 1970) pp. 463–514
17. A. Gruber, J. Gspann: J. Vac. Sci. Technol. B **15**, 2363 (1997)
18. R.J. Schutz: In *VLSI Technology*, ed. by S.M. Sze (McGraw-Hill, New York 1988) pp. 184–234